J. Synchrotron Rad. (1999). **6**, 135–141

XAFS spectroscopy in catalysis research: AXAFS and shape resonances†

Diek Koningsberger,[a]* Barbara Mojet,[a] Jeff Miller[b] and Dave Ramaker[c]

[a]Department of Inorganic Chemistry and Catalysis, Debye Institute, Utrecht University, PO Box 80083, 3508 TB Utrecht, The Netherlands, [b]Amoco Research Center, E-1F, 150 W Warrenville Rd, Naperville, IL 60566, USA, and [c]Chemistry Department, George Washington University, Washington, DC 20052, USA. E-mail: d.c.koningsberger@anorg.chem.ruu.nl

(*Received 9 November 1998; accepted 29 January 1999*)

Two new techniques in X-ray absorption spectroscopy (XAS) have recently been developed which provide previously unobtainable information on supported noble metal catalysts. Atomic X-ray absorption fine structure (AXAFS) provides direct information on the average changes in interatomic potential of the metal particles induced by metal-support effects. Changes in the interatomic potential can now be directly related to changes in catalytic reactivity. Analysis of shape resonances near the X-ray absorption edge provides information on the changes in the nature of the bonding of adsorbates (like hydrogen) to the metal cluster as induced by the properties of the support. The strong decrease in activity of supported platinum clusters for neo-pentane hydrogenolysis with increasing alkalinity of the support can be ascribed to a decrease in ionization potential of the metal particles directly influenced by the alkalinity of the support.

Keywords: AXAFS; interatomic potential; shape resonance; supported metal catalysts; metal-support effects; ionization potential.

1. Introduction

Supported noble metal (like Pt, Pd, Rh) catalysts are used in a large number of commercially important applications, including (de)-hydrogenation, naphtha reforming, isomerization, hydro-cracking, oxidation and automotive exhaust cleaning. Very recently, noble metal (Pd, Pt) particles dispersed in an acidic Y zeolite have been used as catalysts for the production of diesel fuel with low sulfur and aromatic content (van den Berg *et al.*, 1993). Essential for the catalytic performance of these catalysts is the high sulfur tolerance (1000 p.p.m.) of the supported metal particle.

A fundamental study of the sulfur tolerance of small platinum particles dispersed in zeolite LTL (Miller & Koningsberger, 1996) revealed that the acidity of the zeolite support plays a crucial role. Platinum particles dispersed in acidic LTL have a much higher TOF (turnover frequency; catalytic activity per surface platinum atom) than platinum particles dispersed in neutral or alkaline support. Several authors (de Mallmann & Barthomeuf, 1989; Karpinsky *et al.*, 1993; Mojet *et al.*, 1996) have found a pronounced effect of the support on the catalytic activity of noble metal clusters. However, the mechanism of this interaction and, more precisely, how the electronic structure of the metal particles is altered by the support is still unknown.

In this paper a new method is discussed (Mojet *et al.*, 1999; Ramaker *et al.*, 1999) of analysing the L_3 and L_2 X-ray absorption edges of supported platinum particles. The method is based upon (i) subtraction of edges measured with and without chemisorbed hydrogen and (ii) a special aligning procedure in order to remove initial- and final-state effects. By using this procedure electronic and structural information present in the near-edge spectra of platinum can be separated. The anti-bonding state (electronic information) of the Pt–H interaction can be detected and its energy position is dependent on the alkalinity of the support. A Pt–H EXAFS (structural information) is also found to be present in the near-edge structure.

Secondly, this paper will show that information obtained from AXAFS spectra (Ramaker & O'Grady, 1999) is crucial in understanding the metal-support effects in supported metal catalysts. The results show that the Coulomb field of the support oxygen ions, which is determined by the acidity/alkalinity of the support, directly influences the position of the platinum valence *d*-orbitals. The ionization potential of platinum decreases with

† The term 'shape resonance' is used when a particle is temporarily trapped by a potential barrier, and the term 'Fano resonance' is used when the particle is trapped in an autoionizing state. The Fano profile can certainly be used to characterize either case; the only difference is that the first case requires a one-electron decay process, the second a two-electron decay, so that the matrix element for the decay process is different. Since in our case it is a one-electron process and the outgoing electron is temporarily trapped in the potential barrier due to the Pt–H anti-bonding state, we have used the term 'shape resonance'.

increasing alkalinity of the support. *Via* this mechanism the support directly determines the catalytic properties of the supported platinum particles.

2. Experimental

2.1. *Catalysts preparation*

Details of the catalysts preparation are given elsewhere (Ramaker *et al.*, 1999). A saponite support was ion-exhanged with $[Pt(NH_3)_4](NO_3)_2$ and dried at 393 K. This sample will hereafter be denoted as Pt/Sap6, where 6 is the approximate Si/Al ratio. The acidity of an LTL zeolite support was varied by either impregnating a commercial K-LTL zeolite with KNO_3 or exchanging it with NH_4NO_3 to give K/Al ratios ranging from 0.63 to 1.25. Each LTL zeolite was calcined at 498 K. Platinum was added by incipient wetness impregnation with $[Pt(NH_3)_4](NO_3)_2$ (1.0 wt.% Pt) followed by drying at 393 K. The catalysts are designated Pt/LTL(x) where x represents the K/Al molar ratio.

2.2. *XAFS data collection*

The X-ray absorption spectra of the Pt L_3 and L_2 edge of the Pt/LTL catalysts were taken at the SRS (Daresbury) Wiggler Station 9.2, using an Si(220) double-crystal monochromator. The measurements were performed in transmission mode using ion chambers filled with Ar to have an X-ray absorbance of 20% in the first ion chamber and of 80% in the second ion chamber. The monochromator was detuned to 50% maximum intensity at 12 250 eV to avoid higher harmonics present in the X-ray beam. The absorption spectra of the Pt/Sap6 were taken at the ESRF (Grenoble) BM29 station using an Si(111) double-crystal monochromator and with ion chambers with the same type of gas fillings as mentioned above. Samples were pressed into a self-supporting wafer (calculated to have an absorbance of 2.5) and placed in a controlled atmosphere cell (Kampers *et al.*, 1989).

The Pt/Sap6 was dried and reduced in flowing hydrogen at 673 K, and measured under a hydrogen atmosphere at liquid-nitrogen temperature (sample denoted by H–Pt/Sap6). Subsequently, the sample was evacuated at 473 K (1 h) to ensure desorption of all chemisorbed hydrogen. Spectra were taken at LN temperature under continuous evacuation (sample denoted by Pt/Sap6). The Pt/LTL catalysts were reduced in flowing hydrogen at 573 K and measured under a hydrogen atmosphere at LN temperature (sample denoted by H–Pt/LTL). Following reduction, the samples were treated in a helium flow at 573 K to remove chemisorbed hydrogen (sample denoted by Pt/LTL). Further details can be obtained elsewhere (Mojet *et al.*, 1999; Ramaker *et al.*, 1999).

2.3. *EXAFS data analysis*

Standard procedures were used to extract the EXAFS data from the measured absorption spectra. The pre-edge background was approximated by a modified Victoreen curve, normalization completed by dividing by the height of the absorption edge, and the background was subtracted using cubic-spline routines. The EXAFS were analysed using the commercially available data-analysis package *XDAP* (Vaarkamp *et al.*, 1995). The fits were optimized by applying the difference file technique and using phase- and amplitude-corrected Fourier transforms (Koningsberger, 1994). The EXAFS data were fitted in R-space using phase and backscattering amplitudes directly obtained from the experimental EXAFS data for Pt foil and $Na_2Pt(OH)_6$ *via* Fourier filtering (Vaarkamp *et al.*, 1996).

3. Analysis of the near-edge L_2 and L_3 X-ray absorption edges

Hydrogen chemisorption induces a bonding and an anti-bonding orbital as reported by Hammer & Nørskov (1995). The partially occupied platinum surface d-orbitals interact with the hydrogen 1s producing the bonding and anti-bonding Pt–H orbitals. As illustrated in Fig. 1(a), the Pt–H bonding orbital is localized more on the H atom, and the anti-bonding state (AS) is localized more on the surface Pt atoms. Of course, the bonding orbital is occupied so it is not visible in XAS; however, the empty anti-bonding orbital should be evident in XAS.

The different electronic transitions present in the L_2 and L_3 near-edge spectra are schematically viewed in Fig. 1(b). The spin–orbit interaction in both the core and valence levels introduce large differences between the L_3 ($2p_{3/2} \rightarrow$

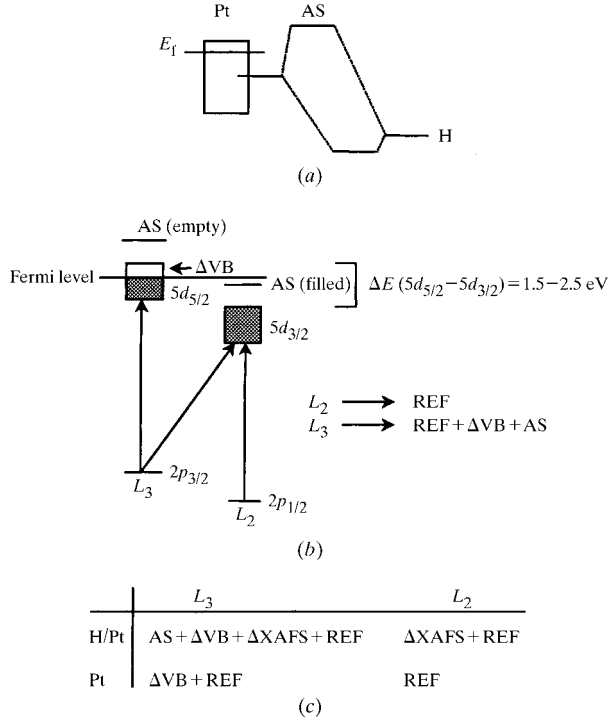

Figure 1
(a) Illustration of MO picture formation of bonding and anti-bonding orbitals derived from a surface Pt orbital and H 1s orbital. (b) Illustration of spin–orbital coupling effects in the X-ray absorption $L_{2/3}$ edge spectra and 5d valence. (c) Matrix summarizing major contributions in each absorption edge.

$5d_{5/2}$,$5d_{3/2}$) and L_2 ($2p_{1/2} \rightarrow 5d_{3/2}$) white lines, both in shape and intensity (the $2p_{3/2}$–$2p_{1/2}$ splitting is ~1709 eV, and the $5d_{5/2}$–$5d_{3/2}$ splitting is ~1.5–2.5 eV) (Mattheiss & Dietz, 1980). The L_3 edge reflects the empty valence band levels (ΔVB) of both the $d_{5/2}$ and $d_{3/2}$ bands, weighted as $d_{5/2}/d_{3/2} = 6$ (Mattheiss & Dietz, 1980); however, the L_2 edge reflects only the $d_{3/2}$ level. For small platinum clusters the $5d_{3/2}$ is believed to be completely filled due to band narrowing relative to platinum bulk; therefore, it is assumed that there is no Pt d valence band (ΔVB) contribution to the L_2 white line. Since the anti-bonding state is primarily localized on the surface Pt atoms, the $5d_{3/2}$ component of the AS is assumed to shift below the Fermi level.

Fig. 1(*c*) summarizes the important contributions that will be visible, based on these assumptions, in the four X-ray absorption edges: L_3 and L_2 edges with and without hydrogen. The L_2-edge spectrum for Pt clusters without chemisorbed hydrogen can be used as the reference (REF), since this spectrum arises from the 'free'-atom absorption and EXAFS contributions and does not contain any valence-band contributions as assumed above. However, the L_3 spectrum of the Pt cluster without hydrogen contains, in addition to REF, the electronic (empty part of the valence band, ΔVB) contribution. The L_2 spectrum for the samples with hydrogen is different from the REF spectrum, because of changes in geometry of the cluster induced by chemisorption of hydrogen (ΔXAFS arising from any additional Pt–H scattering and changes in Pt–Pt and Pt–O scattering). Finally, the L_3 spectrum for the H/Pt sample contains both the geometric (ΔXAFS) and electronic (ΔVB and the chemisorbed hydrogen anti-bonding state, AS) contributions.

By subtracting the L_2 and L_3 edges with and without chemisorbed hydrogen the different contributions (ΔVB, ΔXAFS, AS) can be obtained. First alignment of the L_2 and L_3 edges is necessary in order to remove any initial-state core-level shifts and final-state screening effects. In practice, to remove initial-state effects the L_2 edges are aligned at energy values where the step height of the absorption edges is 0.6. Since the L_3 edges contain different electronic contributions (ΔVB in vacuum, ΔVB + AS in the presence of hydrogen) they have different onsets due to different final-state screening effects. By further alignment of the EXAFS oscillations of the L_3 and L_2 edges for the same sample (with or without hydrogen), all edges are calibrated relative to the sample without chemisorbed hydrogen, thereby correcting for both initial- and final-state screening effects.

The anti-bonding state (AS) is a localized state degenerate with a continuum state (here described by the Pt–H EXAFS wave function) of the platinum particle. This degeneracy gives rise to a shape resonance with the well known Fano-like resonance line shape. Its effect on the scattering cross section $\sigma(E)$ can be related to an EXAFS function $\chi(E)$ *via* the normal expression $\sigma(E) = \mu(E)[1 + \chi(E)]$. It can be shown (Ramaker *et al.*, 1999) that $\chi(E) = (1/k)\ A \sin\varphi\ [(1 - q\varepsilon)/(1 + \varepsilon^2)]$, where A is an amplitude factor, $q = \cot\varphi$ and $\varepsilon = (E - E_{res})/\Gamma$. φ can be related to the usual phase found in EXAFS containing the $2kr$ term and the phase from the absorber and back-scatterer. ε is the normalized energy scale relative to the resonance energy (E_{res}), whereby Γ represents the resonance width. A fit to the experimentally observed AS line shape gives values for E_{res}, Γ, A and φ.

4. Physical principles of atomic XAFS spectroscopy

Ramaker & O'Grady (1999) explained that atomic XAFS is caused by scattering of the outgoing electron against the interatomic potential. This potential is altered from that in the free atom by interactions of electrons in the periphery of the absorber atom with electrons from the neighbouring atom. Of crucial importance is that the AXAFS information can be extracted from the XAFS oscillations after a special procedure for background subtraction. Van Dorssen *et al.* (1999) have recently shown that, by application of this procedure, features due to the Ramsauer Townsend minimum and multiple electron excitations are left in the background, implying that AXAFS can be separated quantitatively from these contributions. In a recently published paper (Ramaker *et al.*, 1998) it has been shown that the Fourier transform of the AXAFS oscillations is proportional to the difference between the embedded potential (V_e) and the truncated free-atom potential (V_{TFA}). The truncated free-atom potential has been defined within the muffin tin approximation. This approximation has been used to describe the interatomic potential, whereby the zero of energy corresponds to V_{int}, the average of the interstitial potentials. The free-atom potential is set to zero when it rises above V_{int}.

5. Results

5.1. *EXAFS*

The EXAFS data analysis is fully described and the results are given and discussed elsewhere (Mojet *et al.*, 1999; Ramaker *et al.*, 1999). The Pt–Pt coordination number of the Pt/Sap6 sample after reduction and evacuation is ~7.3 (approximately 50 atoms per particle). The decrease in Pt—Pt distance by 0.06 Å (from 2.77 to 2.71 Å) indicates that chemisorbed hydrogen indeed desorbs from the surface. The Pt—O distance of 2.2 Å shows that the interfacial Pt atoms are in direct contact with the sapponite support O atoms (Vaarkamp *et al.*, 1996). The metal particles in Pt/LTL are very small, with coordination numbers less that 4.5 (4–6 atoms per particle). The contractions of the Pt—Pt distance for Pt/LTL after handling in helium at 573 K are smaller (~0.02 Å) than for Pt/Sap6 treated in a vacuum at 473 K (~0.06 Å). The long Pt—O distance of ~2.68 Å is in accordance with previous studies on Pt/LTL (Vaarkamp *et al.*, 1993) and is attributed to the presence of interfacial hydrogen. After treatment in helium, only a small contraction occurs in the Pt—Pt and

Pt—O distance for all Pt/LTL samples. The treatment in helium of the Pt/LTL samples leaves He available to physisorb on the platinum surface, resulting in more coordinatively saturated Pt atoms that may counteract the decrease in Pt—Pt distance upon removal of chemisorbed hydrogen. The smaller contractions of the Pt—Pt distance in the Pt/LTL catalysts could occur either because of the incomplete removal of hydrogen or because of the adsorption of He after the hydrogen is desorbed.

5.2. *Analysis of Pt L_2 and L_3 X-ray near-edge spectra*

5.2.1. *Pt/Sap6*. Fig. 2 shows the results after the alignment procedure as discussed in §3. It can be seen that the presence of chemisorbed hydrogen induces large changes in shape and intensity of the near-edge spectra as previously observed (Vaarkamp *et al.*, 1996; Samant *et al.*, 1991; Asakura *et al.*, 1996). Subtracting the different edges from each other leads to the separation of geometric and electronic contributions. The geometric contributions [ΔXAFS = L_2(H/Pt) − L_2(Pt)] as a result of hydrogen chemisorption are displayed in Fig. 3(*a*) (thick dashed line). Comparison of this difference curve with a theoretically calculated (using the *FEFF7* XAFS code) Pt–H EXAFS function using a Pt—H distance of 1.8 Å [thin dashed line in Fig. 3(*a*)] indeed reveals that the ΔXAFS curve is dominated by Pt–H scattering. The combination of geometric and electronic contributions [ΔXAFS + AS = L_3(H/Pt) − L_3(Pt)] is also shown in Fig. 3(*a*) by a solid line. The peak at ~2 eV in this difference curve is due to the AS state and the peak at ~ 8 eV is due to the Pt-H EXAFS.

The electronic contribution (AS) can be isolated by further subtraction of the two difference curves, which are presented in Fig. 3(*b*). The solid line in Fig. 3(*b*) is the result of the subtraction procedure and represents the anti-bonding state AS. It was possible to fit this curve with a Fano-type resonance line shape. The resulting parameters as obtained for the Pt/Sap6 sample are given in Table 1. The theoretical fit was broadened with a 5 eV-wide Gaussian to account for experimental and vibrational broadening.

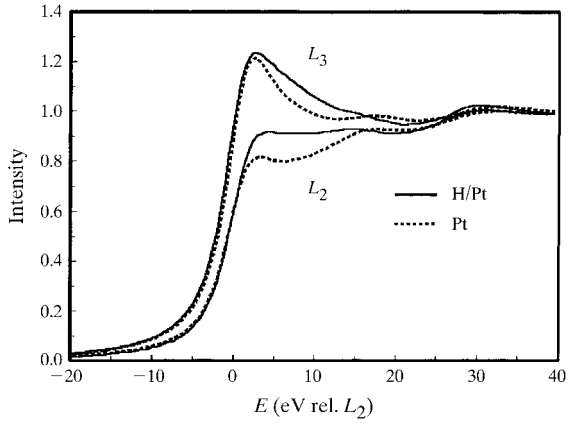

Figure 2
L_3 and L_2 near-edge spectra for H–Pt/Sap6 (reduced at 673 K, hydrogen chemisorbed, solid line) and Pt/Sap6 (evacuated at 473 K, dotted line).

Table 1
Resonance parameters obtained from non-linear least-squares fit of the Fano resonance expression to the hydrogen-induced Fano resonance spectra utilizing $\varphi = \alpha + \beta E_{res}$ with optimal $\alpha = -0.3 \pm 0.1$ and $\beta = 0.38 \pm 0.2$.

Catalyst	A (±0.03)	E_{res} (eV)† (±0.3)	Width, Γ (eV)‡ (±0.4)	φ (calc.) (±0.1)
H–Pt/Sap6	0.15	0.6	1.9	−0.06
H–Pt/LTL(0.63)	0.15	2.0	2.1	0.47
H–Pt/LTL(0.96)	0.04	1.1	3.4	0.10
H–Pt/LTL(1.25)	0.08	−1.2	1.2	−0.76

† Relative to the L_2 absorption edge ‡ Resonance width. A 5 eV Gaussian broadening to account for experimental resolutions was also applied.

5.2.2. *Pt/LTL*. The Pt L_3 and L_2 edges with and without hydrogen show the same trend as observed for the Pt/Sap6 sample. The same alignment and subtraction procedure was used to obtain the geometric (Pt–H EXAFS) and electronic contributions (anti-bonding state AS) for the Pt/LTL series from the absorption-edge spectra. The full analysis of the Pt/LTL samples is given and discussed elsewhere (Ramaker *et al.*, 1999). The acidity of the LTL supports changes from acidic (K/Al = 0.63) to neutral (K/Al = 0.96) to alkaline (K/Al = 1.25). The solid lines in Fig. 4 represent the anti-bonding states of the three samples. The AS line shape systematically changes with the acidic or alkaline properties of the support. The Fano-type profile was again used in a non-linear least-squares fit to the experimental AS line shapes. Also, for the Pt/LTL samples a Gaussian broadening of 5 eV was added to account for the experimental resolution and vibrational broadening. Since φ and Γ are strongly interdependent and the width is quite uncertain because of the large broadening, φ and E_{res} are coupled utilizing the relation $\varphi = \alpha + \beta E_{res}$. All four resonant line shapes (the three LTL and the Sap6 samples) are then fit simultaneously with a total of 14 parameters, *i.e.* E_{res}, Γ and

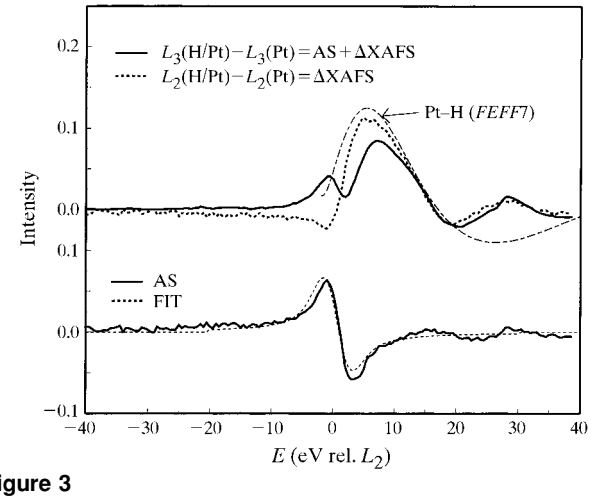

Figure 3
(*a*) L_3 − L_2 (solid line) and L_2 − L_3 (dotted line) difference spectra and Pt–H EXAFS (thin dashed line) as calculated from *FEFF7*. (*b*) Subtraction of the difference spectra (solid line) and Fano line shape fit (dashed line).

A for each resonance (each catalyst), plus α and β. The results are given in Table 1. The dramatic reversal in line shape of the shape resonance with energy is easily reproduced by the Fano profile expression (see Fig. 4, dotted line).

5.3. *AXAFS spectra of Pt/LTL catalysts*

The Fourier transforms (k^3, Δk: 3–13 Å^{-1}) of the AXAFS oscillations of the Pt/LTL catalysts after treatment in He are shown in Fig. 5. The peak position is indeed at low R values (~0.8 Å), which is expected to be at the periphery of the X-ray absorbing atomic atom. The peak position moves to higher R values with increasing alkalinity. At the same time the amplitude of the AXAFS peak systematically decreases. It has to be noted that further separation of the AXAFS from the EXAFS oscillations can be carried out by fitting the first-shell Pt–Pt and Pt–O contributions in R-space and subsequent subtraction of the calculated Pt–Pt and Pt–O EXAFS from the experimental data.

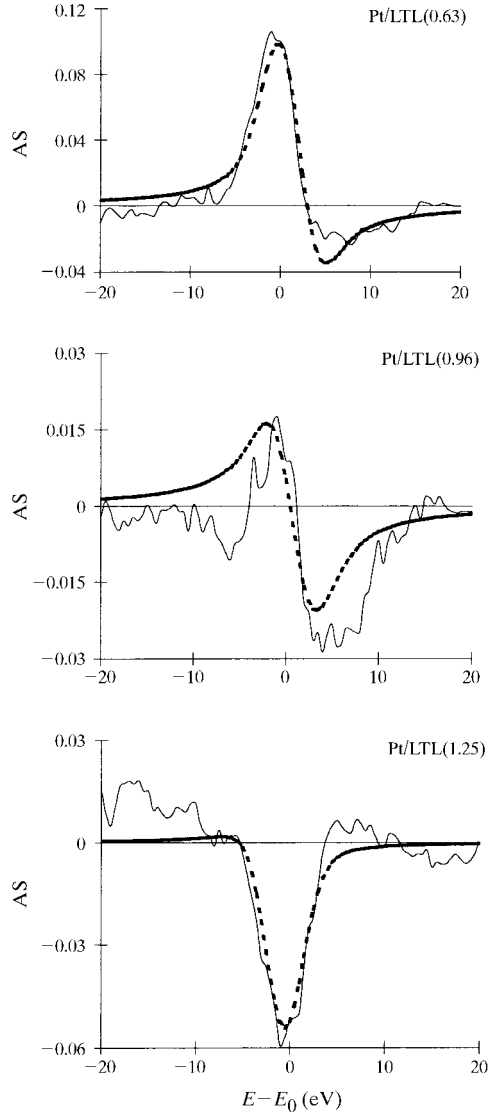

Figure 4
Results of analysis of near-edge spectra of H–Pt/LTL and Pt/LTL: Fano-resonance line shape (*i.e.* AS) for Pt/LTL (solid line) and best fit to resonant line shape with parameters in Table 1.

6. Discussion

6.1. *Hydrogen chemisorption*

The data obtained for Pt/Sap6 and Pt/LTL show that chemisorption of hydrogen leads to changes in structural and electronic properties. The amount of hydrogen, which is removed after treatment in He at 573 K, of the Pt/LTL catalysts is lower than for the Pt/Sap6 sample after evacuation at 473 K. Nevertheless, for all samples the same trends are observed both in the EXAFS and the near-edge spectra.

6.2. *Analysis of Pt L_3 and L_2 near-edge spectra*

6.2.1. *Pt–H EXAFS.* The new procedure of analysing the Pt L_3 and L_2 X-ray absorption edges makes it possible to separate geometric (Pt–H EXAFS) from electronic (AS and ΔVB) contributions in the near-edge energy region. The cross section for scattering of the outgoing electron against hydrogen chemisorbed on the surface of the platinum particles is extremely small at high kinetic energies. In the normal EXAFS regime ($k > 2$ Å^{-1}) the Pt–H scattering is far beyond detection. The theoretically calculated Pt–H EXAFS as shown in Fig. 3(*a*) agrees with the experimentally observed ΔXAFS curve. The deviations as observed beyond 20 eV are due to changes in the normal EXAFS parameters induced by the removal of hydrogen (decrease in Pt—Pt coordination distance). The results of the new analysis procedure show that the presence of hydrogen on the surface of small metal particles can be detected with XAFS spectroscopy. Ramaker & O'Grady (1999) have demonstrated that, by using the same analysis procedure, adsorbates of other low-Z elements can be observed.

6.2.2. *The shape resonance (AS), catalytic properties and other spectroscopic results.* The results of the new align-

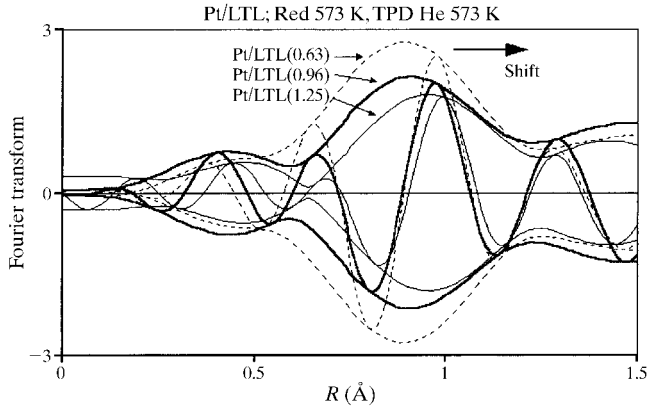

Figure 5
AXAFS spectra (FT, k^3, Δk = 3–13 Å^{-1}) of Pt/LTL catalysts after treatment in He.

ment and subtraction procedure as applied for the Pt/Sap6 sample show that information about the electronic structure can be obtained. The data displayed in Fig. 3(*b*) with a solid line can be fitted with a Fano profile, which strongly indicates that the data represent the Pt–H anti-bonding state (AS) for the Pt/Sap6 sample.

The systematic decrease of the energy difference (position of E_{res}) between the Pt–H anti-bonding state and the Fermi level with increasing alkalinity of the LTL support is striking. The resonance energy, E_{res}, systematically drops in energy from plus to minus with increasing alkalinity for the Pt/LTL system. The negative resonance energy results because the resonance (localized primarily on the Pt atom with the core hole) is pulled down below the Fermi level by the core-hole electron attraction. One has to realise that, consistent with the final-state rule, the values of E_{res} do not reflect the actual energy of the AS in the ground state but in the presence of a core hole. Although the Sap6 support is believed to be considerably more acidic than LTL(0.96), the E_{res} does not fall between LTL(0.63) and LTL(0.96). However, the Pt particles on Sap6 are much larger than for the LTL systems, and the nature of the Pt–H bond may change with particle size due to the increased metallic nature of the larger particles.

The results presented here demonstrate that the electronic structure of the catalytically active surface Pt atoms is indeed directly influenced by the acidity/alkalinity of the support. Earlier work published by our group (Mojet *et al.*, 1994, 1996) showed that the activity per surface platinum atom (TOF = turn-over fequency) for neo-pentane hydrogenolysis on Pt/LTL, Pd/LTL and Pt/SiO_2 catalysts is also strongly influenced by the acid/base properties of the support. Moreover, the decrease in E_{res} (difference in relative positions of the Fermi level and AS state) for the three LTL catalysts has to be related to observations from XPS and FTIR spectroscopy (Mojet *et al.*, 1994, 1996). XPS on Pd/LTL showed a decrease of the Pd 3*d* binding energy with increasing alkalinity (by 1.4 eV from acidic to alkaline Pd/LTL) pointing to a shift of the Fermi level to lower binding energy or a decrease in ionization potential. FTIR showed a systematic decrease in the linear-to-bridge bonded ratio of chemisorbed CO with increasing alkalinity of the support, showing a higher electron backdonation from the *d*-orbitals (van Santen *et al.*, 1987). This increased backdonation, the simultaneous decrease in E_{res} with increasing alkalinity (as shown here), and the shift of the Fermi level to lower binding energy (as found by XPS) reveals a significant influence of the support on the electronic structure of supported metal particles. In the following section an interpretation of the AXAFS data will be given, which will help in a further explanation of the metal-support effect.

6.3. *Influence of the support acidity/alkalinity on the Pt/LTL AXAFS data*

The interatomic potential of the interfacial Pt atoms will be directly influenced by the support oxygen ions. The influence of the support will be averaged over the whole metal particle. The experimental AXAFS data are therefore directly related to an averaged interatomic potential. Oxygen ions of the support will change the shape of the embedded potential of platinum since the interaction with oxygen will delocalize platinum electrons near oxygen. This will result in more 'roll over' of the interatomic potential and consequently a larger difference between V_e and the free-atom potential, *i.e.* increase in the amplitude of the Fourier transform of the AXAFS oscillations. By increasing the negative charge on the support oxygen (as for alkaline supports) the interatomic potential between platinum and oxygen will move up (more electrons contribute to the interatomic potential). This results in less 'roll over' and therefore a lower amplitude of the AXAFS peak. This is schematically shown in Fig. 6.

V_{int} in the muffin tin approximation represents the bottom of the conduction band. The Pd XPS results show that the Fermi level (top of the conduction band) moves to lower binding energy with increasing alkalinity, therefore V_{int} must move to lower binding energy as well. This is also depicted in Fig. 6. The shaded area in Fig. 6 represents the difference between the embedded potential (V_e) and the free-atom potential truncated by V_{int} (V_{TFA}). With increasing alkalinity the shaded area decreases in agreement with the decrease in amplitude of the AXAFS peak which, according to theory, is proportional to the shaded area. The position of the weighted average of the shaded area (indicated in Fig. 6 with an arrow) moves to higher *R* values with increasing alkalinity in agreement with the

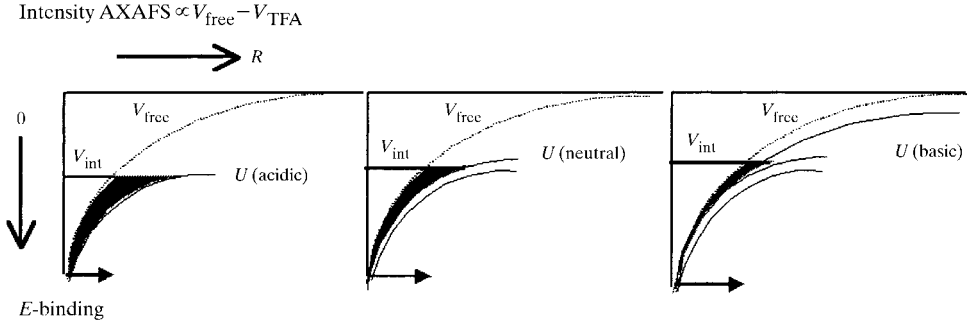

Figure 6
Schematic drawing of the change of interatomic potential in Pt/LTL catalysts as a function of support acidity/alkalinity.

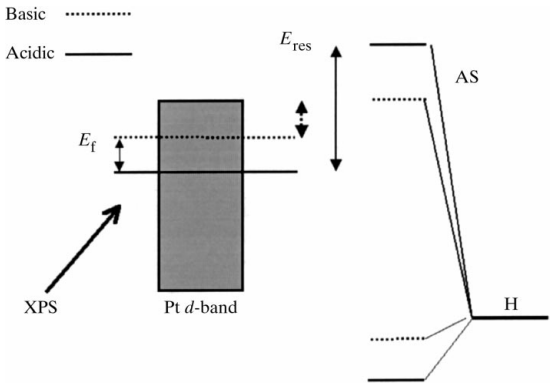

Figure 7
Schematic representation of the change in Pt—H bonding as a function of support acidity/alkalinity.

experimentally observed change of the position of the AXAFS peak in Fig. 5.

6.4. *Electronic model of metal-support interaction*

A combination of the analysis of all platinum XAFS data (L_3 and L_2 near-edge, AXAFS and EXAFS) together with catalytic, XPS and FTIR of chemisorbed CO lead to a model which explains the metal-support interaction as a change in the position of the Pt valence orbitals: decrease of Pt ionization potential with increasing alkalinity. This model is based upon an electrostatic interaction induced by changes in charge density of the support oxygen ions. The consequences of this model for interaction of substrates with the catalytically active surface Pt atoms are schematically shown in Fig. 7 for chemisorption of hydrogen. The H 1*s* orbital is at a fixed energy position. The distance in energy between the H 1*s* orbital and the interacting *d*-orbital increases (based upon XPS and AXAFS) with increasing alkalinity (see Fig. 7). The decrease in energy difference (E_{res}) between the anti-bonding state (AS) and the Fermi level with increasing alkalinity (as observed in this work) implies also a decrease in energy difference between the anti-bonding state (AS) and the interacting *d*-orbital (see also Fig. 7). The consequence of the MO pictorial scheme is that the Pt—H bond weakens with increasing alkalinity.

More research is needed to fully explore the consequences of the model presented here for explaining metal-support interaction. However, this paper demonstrates that AXAFS and shape resonances can provide unique information about metal-adsorbate and metal-support interactions.

References

Asakura, K., Kubota, T., Ichikuni, N. & Iwasawa, Y. (1996). *Stud. Surf. Sci. Catal.* **101**, 911.

Berg, J. P. van den, Lucien, J. P., Germaine, G. & Thielemans, G. L. B. (1993). *Fuel Proc. Tech.* **35**, 119–136.

Hammer, B. & Nørskov, J. K. (1995). *Nature (London)*, **376**, 238.

Kampers, F. W. H., Maas, T. M. J., Van Grondelle, J., Brinkgreve, P. & Koningsberger, D. C. (1989). *Rev. Sci. Instrum.* **60**, 2645.

Karpinsky, Z., Dahdi, S. N. & Sachtler, W. M. H. (1993). *J. Catal.* **141**, 337.

Koningsberger, D. C. (1994). *Appl. Solid State Phys. Chem.* **2**, 213–214.

Mallmann, A. de & Barthomeuf, D. (1989). *Stud. Surf. Sci. Catal.* **46**, 429.

Mattheis, L. F. & Dietz, R. E. (1980). *Phys. Rev. B*, **22**(4), 1663.

Miller, J. T. & Koningsberger, D. C. (1996). *J. Catal.* **162**, 209.

Mojet, B. L., Kappers, M. J., Miller, J. T. & Koningsberger, D. C. (1996). *Stud. Surf. Sci. Catal.* **101**B, 1165.

Mojet, B. L., Kappers, M. J., Muijsers, J. C., Niemantsverdriet, J. W., Miller, J. T., Modica, F. S. & Koningsberger, D. C. (1994). *Stud. Surf. Sci. Catal.* **84**, 909.

Mojet, B. L., Miller, J. T., Ramaker, D. E. & Koningsberger, D. C. (1999). *J. Catal.* Submitted.

Ramaker, D. E., Mojet, B. L., Garriga Oostenbrink, M. T., Miller, J. T. & Koningsberger, D. C. (1999). Submitted.

Ramaker, D. E., Mojet, B. L., Koningsberger, D. C. & O'Grady, W. E. (1998). *J. Phys. Condens. Matter*, **10**, 1–18.

Ramaker, D. E. & O'Grady, W. (1999). *J. Synchrotron Rad.* **6**, 800–802.

Samant, M. G. & Boudart, M. (1991). *J. Phys. Chem.* **95**, 4070.

Santen, R. A. van (1987). *J. Chem. Soc. Faraday Trans.* **83**, 1915.

Vaarkamp, M., Linders, J. C. & Koningsberger, D. C. (1995). *Physica B*, **159**, 208–209.

Vaarkamp, M., Miller, J. T., Modica, F. S. & Koningsberger, D. C. (1996). *J. Catal.* **163**, 294.

Vaarkamp, M., Modica, F. S., Miller, J. T. & Koningsberger, D. C. (1993). *J. Catal.* **144**, 611–626.

Van Dorssen, G. E., Koningsberger, D. C. & Ramaker, D. E. (1999). *Phys. Rev. B.* Submitted.